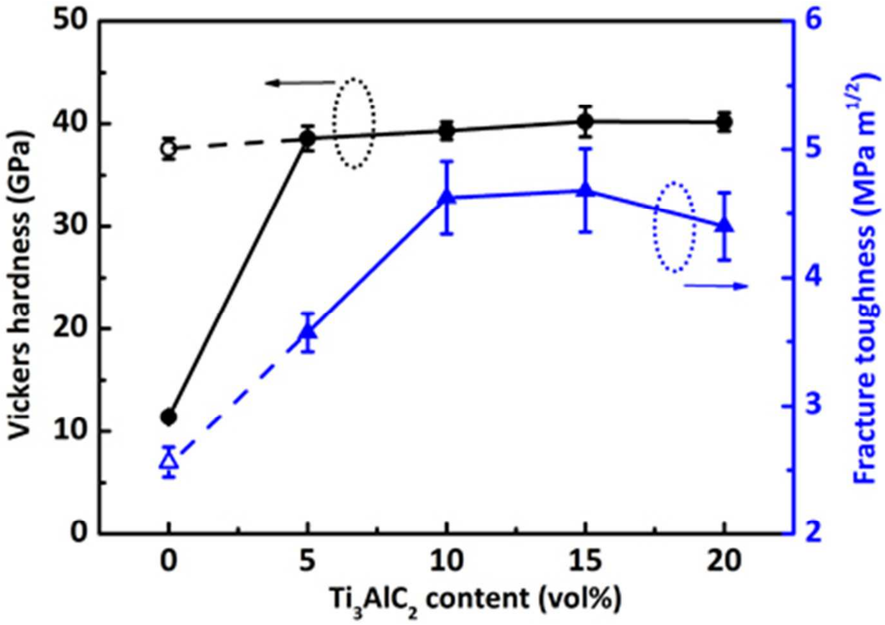

Ti3AlC2 was chosen as a novel sintering aid to fabricate dense B4C ceramics with high mechanical properties.
39x26mm (300 x 300 DPI)

RSC Advances

ARTICLE

Enhancement of Sinterability and Mechanical Properties of B_4C Ceramics Using Ti_3AlC_2 as a Sintering Aid

Received 00th January 20xx,
Accepted 00th January 20xx

DOI: 10.1039/x0xx00000x

www.rsc.org/

Y. Q. Tan,[a] C. Chen,[a] F. Z. Li,[a] H. B. Zhang,[a, †] G. J. Zhang[b, †] and S. M. Peng[a, †]

Boron carbide (B_4C) ceramics are currently the leading control rod materials in fast nuclear reactors and promising high temperature structural materials. However, several drawbacks such as poor sinterability and low toughness seriously limit their wide applications. In order to enhance the sinterability and mechanical properties of B_4C ceramics, titanium aluminum carbide (Ti_3AlC_2) was chosen as a new efficient sintering aid to densify B_4C ceramics using spark plasma sintering. Fully dense B_4C ceramics were obtained at a lower sintering temperature of 1500°C by adding a small amount of Ti_3AlC_2. Meanwhile, the mechanical properties were enhanced remarkably. For B_4C ceramics sintered with 15 vol% Ti_3AlC_2, optimized mechanical properties were obtained with Vickers hardness of 40.2 GPa and indentation fracture toughness of 4.7 MPa•m$^{1/2}$. These results indicate that Ti_3AlC_2 can be used as a novel sintering aid for the densification of B_4C ceramics.

Introduction

Boron carbide (B_4C) ceramics are excellent structural materials due to their low density (2.52 g/cm^3), high Yong's modulus (~440 GPa) and high Vickers hardness (~30 GPa),[1,2] which make B_4C ceramics excellent candidates for light-weight body armors. B_4C ceramics also have great potential for high temperature applications in non-oxidizing environment owing to their high melting point and good chemical stability. Besides, B_4C ceramics are important functional materials due to the neutron absorption ability of isotope ^{10}B which owns a high neutron absorption cross-section over a wide range of neutron energies. Because of their high B content, good chemical inertness and good mechanical properties, B_4C ceramics are extensively used in the nuclear reactors as control rods, shielding materials and as neutron detectors. Currently, they are the leading control rod materials in liquid-metal-cooled fast breeder reactors (LMFBR) and boiling water reactors (BWR).[3]

However, there exist several major restrictions for the wide applications of B_4C ceramics as both structural and functional materials: a) poor sinterability due to the highly covalent bonding and the associated low diffusion mobility; b) low machinability due to high hardness and low electrical conductivity; c) relatively low strength and toughness.[1] Further, as control rod materials in nuclear reactors, B_4C ceramics often experience serious cracking when subjected to thermal stresses and helium gas due to their intrinsic low thermal conductivity, low toughness and poor thermal shock resistance.[4]

The poor sinterability makes the preparation and processing of B_4C ceramics rather complicated and energy-consuming. The relatively low toughness and low thermal conductivity of B_4C ceramics could influence the lifetime of control rods and raise safety problems to the nuclear reactors.[5] Thus it is essential to lower the sintering temperature and enhance the mechanical properties of B_4C ceramics for wider applications and the extension of lifetime of control rods in nuclear reactors. Many efforts have been paid to lower the sintering temperature of B_4C ceramics and improve their mechanical properties. For the reduction of sintering temperature, carbon (C),[6-8] metallic phase such as aluminium (Al),[9-11] silicon (Si),[12,13] and titanium (Ti),[14] oxides such as alumina (Al_2O_3) and rare earth oxides,[15,16] as well as borides[17] were commonly chosen as sintering aids. C is effective in reducing the sintering temperature of pressureless sintered B_4C because C can remove the oxide layer of B_4C particles and enhance the diffusion at the grain boundaries.[6-8] The other sintering aids mentioned above generally form liquid phase due to their lower melting points and thus promote densification of B_4C ceramics significantly.[9-17] Although these sintering aids can facilitate sintering of B_4C ceramics at a much lower temperature, in most cases, no remarkable improvements on mechanical properties of B_4C ceramics were achieved. Generally, the residual carbon or metallic phases at the grain boundaries generally deteriorate the unique properties of hard ceramics. Moreover, abnormal grain growth caused by liquid phase during sintering could lead to lower toughness of ceramics. In order to increase the strength and toughness of B_4C ceramics, several additives have been explored such as TiB_2, ZrB_2 and SiC,[11,18-22] among which TiB_2 is the most

---

[a] Innovation Research Team for Advanced Ceramics, Institute of Nuclear Physics and Chemistry, China Academy of Engineering Physics, Mianyang, 621900, China.
[b] Shanghai Institute of Ceramics, Chinese Academy of Sciences, Shanghai 200050, China.
† Corresponding authors Email: hbzhang@caep.cn, gjzhang@mail.sic.ac.cn, pengshuming@caep.cn.

extensively studied. The B_4C-TiB_2 composites can be obtained by direct mixing of B_4C and TiB_2,[11] or by in situ reaction sintering between B_4C and TiC or TiO_2 and C.[18-20] Besides, carbon nanotube (CNT)[9] and carbon nanofiber (CNF)[23] reinforced B_4C ceramics were also reported. The introduction of TiB_2, CNT or CNF could result in a remarkable increase of the mechanical properties of B_4C ceramics. Generally, B_4C-TiB_2 composites show an improved fracture toughness in the range of 3-6 MPa•$m^{1/2}$ depending on the amount of TiB_2 and different sintering methods.[11,18-20] B_4C-CNF composite was reported to exhibit an extremely high fracture toughness of 7.5 MPa•$m^{1/2}$ when the volume fraction of CNF was 15%.[23] However, the enhancement of sinterability for B_4C ceramics is quite limited. The sintering temperature of B_4C-TiB_2 composites still needs to be around 2000°C and above by reaction hot-pressing of B_4C, TiO_2 and C powders.[19]

In order to enhance the sinterability and mechanical properties of B_4C ceramics simultaneously, titanium aluminum carbide (Ti_3AlC_2), a typical member of the MAX phases, was chosen as a sintering aid to prepare dense B_4C ceramics in this study. The densification was carried out by spark plasma sintering which is an effective way to fabricate dense nanostructured ceramics. The influence of Ti_3AlC_2 content on the sinterability and mechanical properties of B_4C ceramics was systematically studied.

Experimental

B_4C powders (Grade HS, H. C. Starck GmbH, Germany) and Ti_3AlC_2 powders (>99%, Forsman, China) were used as starting materials. Figure 1 shows the microstructures of these two raw materials. The B_4C powder has a uniform grain size distribution with an average particle size of 0.5 μm and the Ti_3AlC_2 powder used in this study shows a broad grain size distribution from 0.5 μm to about 10 μm, as shown in Fig.1. B_4C and Ti_3AlC_2 powders were mixed according to the formula of B_4C-x vol% Ti_3AlC_2 with x=0, 5, 10, 15 and 20. The mixed powders were ball-milled for 10 h with SiO_2 balls using ethanol as a ball-milling media. After ball-milling, the mixed powders were dried and then put into a carbon die with an inner diameter of 15 mm. B_4C-x vol% Ti_3AlC_2 mixtures were sintered in vacuum using an SPS furnace (Labox-325, Japan) for 3 minutes at different temperatures. The heating rate is 100°C/min and a uniaxial pressure of 80 MPa was applied during sintering.

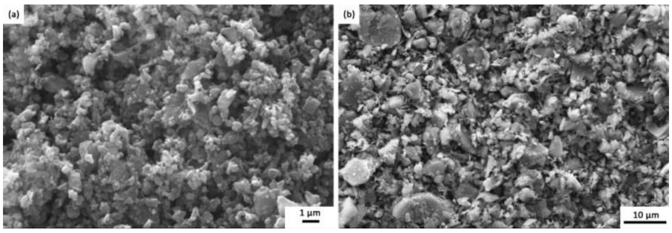

Figure 1. Microstructure of (a) B_4C and (b) Ti_3AlC_2 powders.

The density of the sintered samples was measured by the Archimedes's method. Crystalline phases were characterized by X-ray diffraction (XRD). The microstructure of the specimens was observed using scanning electron microscopy (SEM) with an energy-dispersive X-ray (EDX) analyser. In order to measure the Vickers hardness (H_V) and fracture toughness (K_{IC}), specimens were first polished with diamond slurry. Hardness was determined by the Vickers diamond indentation method using the following equation:

$$H_v = 1.854 \times 10^9 \cdot P/d^2 \qquad (1)$$

where P is the indentation load (9.8 N in this study) on the polished surface and d is the average diagonal length of the Vickers indentation. Indentation fracture toughness values of the specimens were semiquantitatively estimated from observed corner cracks and calculated Vickers hardness using the Anstis equation:

$$K_{IC}=0.016\cdot(E/H_v)^{1/2}\cdot(P/c^{3/2}) \qquad (2)$$

where E is the Yong' s modulus and c is the half-length of cracks formed by the indentation (also induced with a 9.8 N load in this study).[24]

Results and discussion

Figure 2 shows the density of B_4C ceramics sintered with different amount of Ti_3AlC_2 at 1500°C. The density of monolithic B_4C ceramics spark plasma sintered at 1500°C is only 2.02 g/cm^3, which is about 80.1% of the theoretical density. When 5 vol% Ti_3AlC_2 was added, the density of B_4C increased dramatically to 2.69 g/cm^3. Further increase in Ti_3AlC_2 content did not bring to any appreciable density increase. 5 vol% of Ti_3AlC_2 was therefore enough to obtain a fully dense B_4C ceramic at 1500°C. When the sintering temperature was increased to 1600°C, the relative density of monolithic B_4C ceramics increased to 98.0%. This indicates that the lowest sintering temperature for fully dense B_4C ceramics is at least 100°C lower when spark plasma sintered using Ti_3AlC_2 as a sintering aid, which suggests that Ti_3AlC_2 is quite effective in lowering the sintering temperature of B_4C ceramics

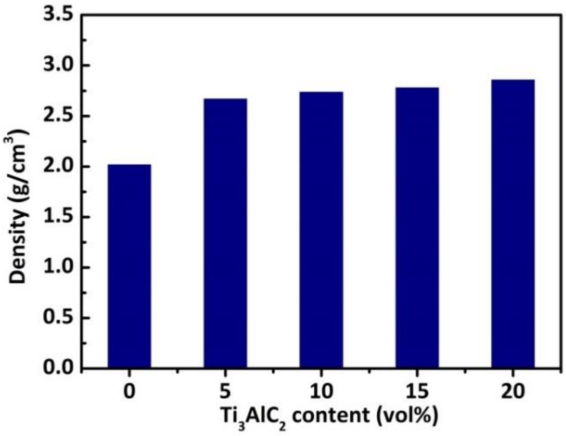

Figure 2. Density of B_4C ceramics with different amount of Ti_3AlC_2 content sintered at 1500°C.

The phase composition of B_4C ceramics sintered with different amount of Ti_3AlC_2 was examined by XRD analysis and the results are shown in Fig. 3. For monolithic B_4C ceramics, only diffraction peaks of single phase B_4C were detected. B_4C ceramics sintered with Ti_3AlC_2 show several additional diffraction peaks besides those corresponding to B_4C. However, no Ti_3AlC_2 diffraction peaks were observed, demonstrating that Ti_3AlC_2 decomposed completely at high temperature. The existence of TiB_2 can be identified by the diffraction peaks labelled in Fig.4, and it can be seen that the intensity of the main TiB_2 diffraction peak around 45° increases gradually with the increase of Ti_3AlC_2 content. A broad peak around 26° indicates the existence of C and its intensity also increases with the increase of Ti_3AlC_2 amount. Further, a small peak around 33° which belongs to Al_2OC phase was observed for all B_4C ceramics sintered with Ti_3AlC_2. For B_4C ceramics sintered with 20 vol% Ti_3AlC_2, one more set of additional diffraction peaks was detected. An accurate peak matching revealed that it corresponds to the Al-B-C phase $Al_8B_4C_7$, which was also observed in previous B_4C ceramics sintered using Al as sintering aid.[7,13] Based on the XRD results and previous studies, it can be summarized that the Ti_3AlC_2 first decomposed according to the following reaction:[25]

$$Ti_3AlC_2 \rightarrow 3TiC_{2/3} + Al \qquad (3)$$

Then $TiC_{2/3}$ and Al reacted with B_4C respectively during sintering according to the following reactions:[26]

$$3B_4C + 6TiC_{2/3} \rightarrow 6TiB_2 + 7C \qquad (4)$$

$$8Al + B_4C + 6C \rightarrow Al_8B_4C_7. \qquad (5)$$

As to the Al_2OC phase, it is suggested that the oxygen may come from the oxide layer of B_4C particles. Generally, the outer surface of B_4C fine particle is covered by an oxide layer of B_2O_3, which is one reason for the low sinterability of B_4C ceramics.[1,7] In this study, it is suggested that Al decomposed from Ti_3AlC_2 and the residual C from the above reactions can remove this oxidized layer and form Al_2OC phase according to the following reactions:

$$2Al + B_2O_3 \rightarrow Al_2O_3 + 2B \qquad (6)$$

$$Al_2O_3 + 3C \rightarrow Al_2OC + 2CO \qquad (7)$$

which were also reported in previous studies.[27] The reaction between B_4C and Ti_3AlC_2 during sintering could also give rise to fine grains of B_4C ceramics because of the lower temperature.

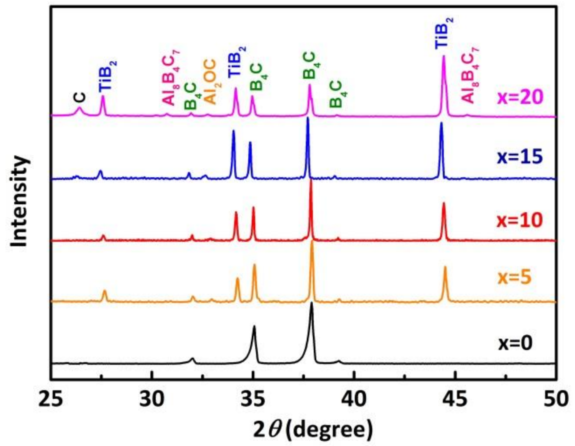

Figure 3. XRD profile of B_4C ceramics sintered at 1500°C with different amount of Ti_3AlC_2 additive.

Figure 4 shows the microstructures observed in the polished surface of B_4C ceramics sintered with different amount of Ti_3AlC_2 and the typical EDS spectra of B_4C ceramics sintered with 15 vol% Ti_3AlC_2. Figs.4 (a) and (b) are polished surfaces of monolithic B_4C ceramics sintered at 1500°C and 1600°C respectively; Figs.4 (c)-(f) correspond to B_4C ceramics sintered at 1500°C with 5, 10, 15 and 20 vol% Ti_3AlC_2 respectively. Monolithic B_4C ceramic sintered at 1500°C shows a porous microstructure, which is consistent with its low density. When sintered at 1600°C, B_4C ceramic becomes much denser as shown in Fig.4 (b). All the B_4C ceramics sintered at 1500°C with Ti_3AlC_2 as sintering aid show quite dense microstructures. With the addition of Ti_3AlC_2, a white contrasted phase uniformly dispersed in the B_4C matrix starts to appear, indicating the presence of second phases. The size of these white spots varies from 0.5 µm to about 10 µm, which is consistent with the size distribution of raw Ti_3AlC_2 powders. The volume fraction of these white spots was estimated from the polished surfaces using the ImageJ software and it is calculated to be 6.2%, 13.8%, 17.4% and 24.9% for B_4C ceramics sintered with 5, 10, 15 and 20 vol% Ti_3AlC_2 respectively. These values are roughly consistent with the volume fractions of the secondary phases proposed by equations (3)-(5) for B_4C ceramics sintered with different amount of Ti_3AlC_2.

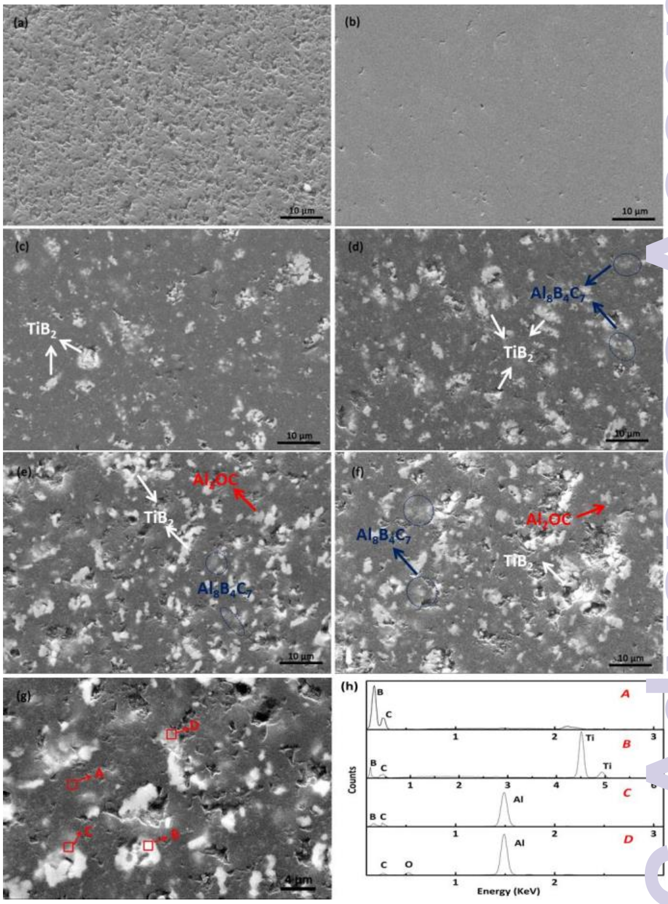

Figure 4. Polished surfaces of B_4C ceramics sintered with different amount of Ti_3AlC_2 content and the related EDS spectra. (a) monolithic B_4C sintered at 1500°C; (b) monolithic B_4C sintered at 1600°C; (c) B_4C-5 vol% Ti_3AlC_2; (d) B_4C-10 vol%

Ti_3AlC_2; (e) B_4C-15 vol% Ti_3AlC_2; (f) B_4C-20 vol% Ti_3AlC_2; (g) B_4C-15 vol% Ti_3AlC_2 at higher magnification; (h) EDS spectra of areas shown in Fig. (g).

In order to present a better understanding of the distribution of different phases in the B_4C matrix, quantitative analysis of the second phases was done by SEM with EDS analyser on the polished surface of B_4C ceramics sintered with different amount of Ti_3AlC_2. As shown in Fig.4, the grey area is the main B_4C phase, and the white spots indicated with white arrows are TiB_2 according to the EDS analysis (Fig.4(h)). Besides the white spots, there also exist some white areas which have no clear boundaries as indicated in the blue circles of Figs.4 (c)-(f). The EDS spectrum demonstrates that they are Al-B-C phases (Fig.4(h)), and referring to the XRD results they should be $Al_8B_4C_7$. It was supposed that Al originally existed at the brighter contrasted areas, and then the molten Al diffused into surroundings during sintering. The light grey spots indicated with red arrows in Figs.4 (e) and (f) and area D in Fig.4 (g) are Al-O-C phase, presumably Al_2OC (Fig.4(h)).

From the above experimental results, it can be summarized that the mechanisms for the enhancement of sinterability of B_4C ceramics using Ti_3AlC_2 as a sintering aid are many-sided. Firstly, Ti_3AlC_2 can decompose into Al and $TiC_{2/3}$ at high temperature, which has been confirmed by previous study.[25] The Al decomposed from Ti_3AlC_2 can form liquid phase at high temperature and promote sintering effectively. Secondly, Al can remove the oxide layer of B_4C particles. The elimination of oxides layer on the surface of initial B_4C powders allows direct contact between B_4C particles, permitting sintering to initiate at significantly lower temperature,[1] thereby accelerating the densification of B_4C. Thirdly, the in situ reaction sintering between B_4C and $TiC_{2/3}$ facilitates mass transfer in the aggregate and the enhancement of mass transport could allow the densification to occur at lower temperatures where the grain growth is still limited. The residual C produced by the reaction between B_4C and $TiC_{2/3}$ could further removes the oxide layer. Besides, it has been confirmed that the presence of TiB_2 could result in lowering of activation energy for sintering of B_4C through various machnisms.[28] The increased sinterability has been reported in the B_4C-TiB_2 composites through reaction hot-pressing of B_4C and TiC.[29] Therefore, the improved sinterability of B_4C ceramics using Ti_3AlC_2 as sintering aid is a consequence of liquid phase sintering, removal of oxide layer and in situ reactive sintering. The reactive sintering and the presence of TiB_2 and C could also inhibit grain growth effectively, thereby giving rise to fine and uniform grain size distributions.

Figure 5 shows the typical optical micrographs of the Vickers hardness indents and the induced cracks of B_4C ceramics sintered with different amounts of Ti_3AlC_2. Figs.5 (a) and (b) correspond to monolithic B_4C sintered at 1500°C and 1600°C respectively, and Figs.5 (b)-(d) correspond to B_4C ceramics sintered at 1500°C with 5, 10, 15 and 20 vol% Ti_3AlC_2 respectively. It can be seen that all ceramics show clear indentations. Monolithic B_4C ceramics exhibit long and straight cracks induced by the indentation. In case of B_4C ceramics sintered with Ti_3AlC_2, the cracks become shorter and more curved and the indentation becomes smaller.

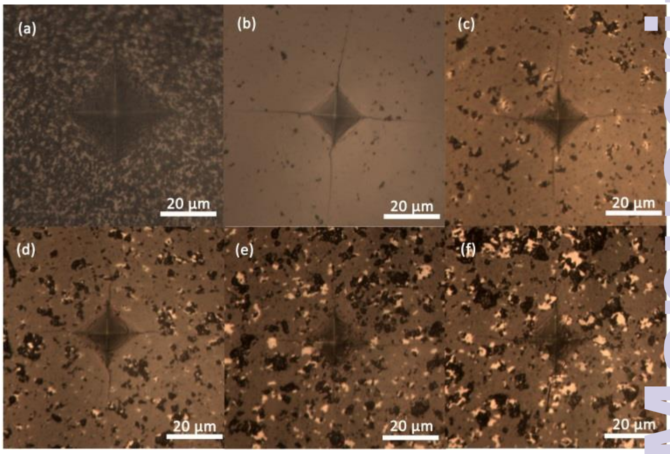

Figure 5. Optical micrographs of the Vickers hardness indents and the induced cracks of (a) monolithic B_4C sintered at 1500°C; (b) monolithic B_4C sintered at 1600°C; (c) B_4C-5 vol% Ti_3AlC_2; (d) B_4C-10 vol% Ti_3AlC_2; (e) B_4C-15 vol% Ti_3AlC_2; (f) B_4C-20 vol% Ti_3AlC_2.

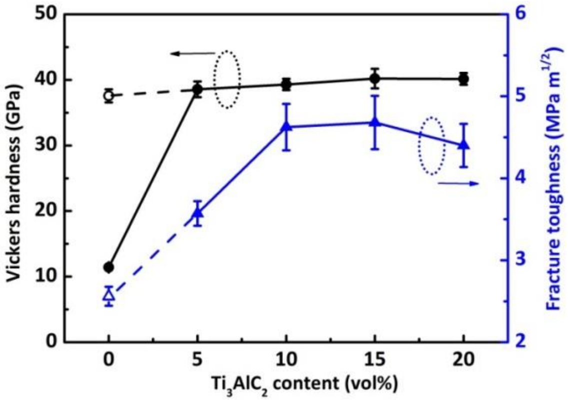

Figure 6. Variations of Vickers hardness and fracture toughness of B_4C ceramics with the amount of Ti_3AlC_2 additive, hollow markers refer to monolithic B_4C sintered at 1600°C.

The Vickers hardness and indentation fracture toughness of all these B_4C ceramics were calculated according to the length of the indentations and the induced cracks, and the results are shown in Fig. 6. The filled symbols represent B_4C ceramics sintered at 1500°C with different amount of Ti_3AlC_2, while the open symbols represent monolithic B_4C ceramics sintered at 1600°C. Monolithic B_4C ceramic sintered at 1500°C shows low Vickers hardness of 12 GPa due to its high porosity. The Vickers hardness of monolithic B_4C ceramic increases dramatically to 37.6 GPa when sintered at 1600°C. In case of B_4C ceramics sintered with Ti_3AlC_2, only a slight increase of Vickers hardness is obtained compared to fully dense monolithic B_4C ceramics. With increasing the amount the Ti_3AlC_2, the Vickers harness of B_4C ceramics keeps almost the same around 40 GPa, which is higher than most of the B_4C ceramics and B_4C-TiB_2 composites reported[1,11] and close to the values of superhard B_4C–ZrB_2 ceramics.[30,31] Porosity and grain size are two most important factors that can influence the Vickers hardness of B_4C ceramics. In this study, except the monolithic ceramic sintered at 1500°C, all the other B_4C ceramics have high density with only negligible porosity. Besides, SPS could supress the grain growth effectively, especially when using Ti_3AlC_2 as a sintering aid. Thus the low porosity and fine grain size (around 0.5 µm) give rise to high Vickers hardness in this study. Different from the Vickers hardness, the fracture toughness of B_4C ceramics changes dramatically with the increase of Ti_3AlC_2 content. For dense monolithic B_4C ceramics, the indentation fracture toughness is only 2.32 MPa•m$^{1/2}$, which is in good consistency with previous reports.[1,11] It increases gradually with increasing Ti_3AlC_2 content and a maximum value of 4.7 MPa•m$^{1/2}$ is achieved for B_4C ceramics sintered with 10 and 15 vol% Ti_3AlC_2. The increase of indentation fracture toughness can be ascribed to following two main factors: a well sintered fine-grained B_4C matrix and uniformly distributed TiB_2 particles. The different thermal expansion coefficients of TiB_2 (α=8.7×10^{-6} K^{-1}) and B_4C (α=5.7×10^{-6} K^{-1}) generate residual stress around TiB_2 particles during cooling and this residual stress gives rise to the microcracks and thus the crack deflection.[20] In this study, the propagation of cracks was hindered by the dispersion of TiB_2 particles and the higher fracture toughness in B_4C ceramic sintered with 10 and 15vol% Ti_3AlC_2 can be explained by the crack deflection by TiB_2 particles, as demonstrated in Fig. 7. With further increase of Ti_3AlC_2 content to 20 vol%, the fracture toughness of B_4C ceramics decreases slightly. The increase of Al-rich phases is one possible reason. For B_4C ceramics sintered with 20 vol% Ti_3AlC_2, some aggregation of TiB_2 particles are shown in Fig.4 (f), and the aggregation of TiB_2 phases could be responsible for the decrease of fracture toughness.

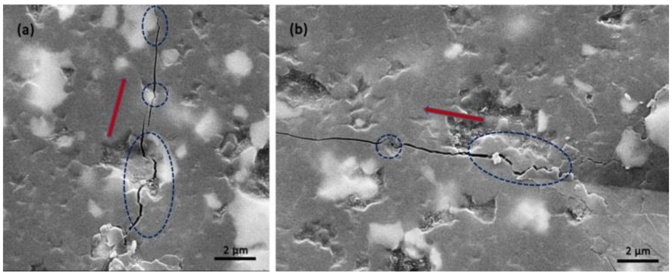

Figure 7. Demonstration of crack deflection in B_4C ceramics sintered with (a) 15 vol% and (b) 20 vol% Ti_3AlC_2, the arrows indicate the crack propogation directions.

Conclusions

Fully dense B_4C ceramics were obtained at a lower sintering temperature using Ti_3AlC_2 as a novel sintering aid in this study, meanwhile their mechanical properties were enhanced. The B_4C ceramics sintered with 15 vol% Ti_3AlC_2 exhibits the maximized mechanical properties with H_v=40.2 GPa and K_{IC}=4.7 MPam$^{1/2}$. The mechanisms for the enhancement of sinterability include liquid phase of aluminium decomposed from Ti_3AlC_2 at high temperatures, removal of surface oxide layer B_2O_3 by C and Al and reaction sintering between B_4C and $TiC_{2/3}$. The enhancement of mechanical properties was mainly attributed to grain refinement and crack deflections owing to the presence of TiB_2 particles.

Acknowledgements

Haibin Zhang is grateful to the foundation by the Recruitment Program of Global Youth Experts and the Youth Hundred Talents Project of Sichuan Province. This work is supported by the National Natural Science Foundation of China (Grant No. 91326102), the Science and Technology Development Foundation of China Academy of Engineering Physics (Grant No. 2013A0301012), and Science and Technology Innovation Research Foundation of Institute of Nuclear Physics and Chemistry.

References

1 A. K. Suri, C. Subramanian, J. K. Sonber and T. S. R. Ch. Murthy, *International Materials Reviews*, 2010, **55**, 1.
2 V. Domnich, S. Reynaud, R. A. Haber and M. Chhowalla, *J. Am. Ceram. Soc.*, 2011, **94**, 3605.
3 F. Thevenot, *J. Eur. Ceram. Soc*., 1990, **6**, 205.
4 T. Stoto, N. Housseau, L. Zuppiroli and B. Kryger, *J. Appl. Phys*., 1990, **68**, 3198.
5 T. Maruyama, *J. Technol. Assoc. Refract. Jpn*., 2010, **30**, 80.
6 K. A. Schwetz and W. Grellner, *J. Less Comm. Met.*, 1981, **82**, 37.
7 B. Y. Yin, L. S. Wang and Y. C. Fang, *J. Chin. Ceram. Soc.*, 2001, **29**, 68.
8 H. Lee and R. F. Speyer, *J. Am. Ceram. Soc*., 2003, **86**, 1468.
9 T. Kobayashi, K. Yoshida and T. Yano, *J. Nucl. Mater*., 2013, **440**, 524.
10 C. H. Danny, J. P. Aleksander, A. A. Ilhan and E. S. William, *J. Am. Ceram. Soc.*, 1989, **72**, 775.
11 M. Mashhadi, E. Taheri-Nassaj, M. Mashhadi and V. M. Sglavo, *Ceram. Inter*., 2011, **37**, 3229.
12 F. Ye, Z. Hou, H. Zhang and L. Liu, *J. Am. Ceram. Soc*., 2010, **93**, 2956.
13 C. Xu, H. Zeng, G. Zhang, *Int. Journal of Refractory Metals and Hard Materials*, 2013, **41**, 2.
14 R. Telle and G. Petzow, *Powder Metall*., 1986, 2, 1155.
15 C. H. Lee and C. H. Kim, *J. Mater. Sci*., 1992, **27**, 6335.
16 K. Y. Xie, M. F. Toksoy, K. Kuwelkar, B. Zhang, J. A. Krogstad, R. A. Haber and K. J. Hemker, *J. Am. Ceram. Soc*., 2014, **97**, 3710.
17 S. Yamada, K. Hirao, Y. Yamachi and S. Knzaki, *J. Mater. Sci. Lett*., 2002, **21**, 1445.
18 A. Goldstein, Y. Yeshurun and A. Goldenberg, *J. Eur. Ceram. Soc.*, 2007, **27**, 695.
19 S. Yamadaa, K. Hiraob, Y. Yamauchib and S. Kanzakib, *J. Eur. Ceram. Soc*., 2003, **23**, 1123.
20 V. Skorokhod and V. D. Krstic, *J. Mater. Sci. Lett.*, 2000, **19**, 237.
21 A. Goldstein, Y. Geffen and A. Goldenberg, *J. Am. Ceram. Soc*., 2001, **84**, 642.
22 Z. Zhang, X. Du, Z. Li, W. Wang, J. Zhang and Z. Fu, *J. Eur. Ceram. Soc.*, 2014, **34**, 2153.
23 K. Hirota, Y. Nakayama and S. Nakane, US Patent, US 2010/0311561 A1.
24 G. R. Anstis, P. Chantikul, B. R. Lawn and D. B. Marshall, *J. Am. Ceram. Soc*., 1981, **64**, 533.

25 L.Y. Zheng, F.Z Li and Y.C. Zhou, *J. Am. Ceram. Soc*., 2012, **95**, 2028.

26 T. Wang and A. Yamaguchi, *J. Mater. Sci. Lett.,* 2000, **19**, 1245.

27 Y. Gao, Z. Huang, M. Fang, Y. Liu, S. Huang and X. Ouyang, *Powder Technol*., 2012, **226**, 269.

28 V. V. Skorokhod, M. D. Vlajic and V. D. Krstic, *Mater. Sci. Forum*, 1998, **282-283**, 219.

29 J. Deng and J. Sun, *Ceram. Inter*., 2009, **35**, 771.

30 W. G. Fahrenholtz, E. W. Neuman, H. J. Brown-Shaklee and G. E. Hilmas, *J. Am. Ceram. Soc.*, 2010, **93**, 3580.

31 J.Zou, S. Huang, K. Vanmeensel, G. Zhang, J. Vleugels and O. Van der Biest, *J. Am. Ceram. Soc*., 2013, **96**, 1055.